

MARGIN: Margin-Aware Regularized Geometry for Imbalanced Vulnerability Detection

Yuteng Zhang, Huifang Ma, *Member, IEEE*, Jiahui Wei, Qingqing Li, and Yafei Yang

Abstract—Software vulnerability detection is critical for ensuring software security and reliability. Despite recent advances in deep learning, real-world vulnerability datasets suffer from two severe challenges: frequency imbalance and difficulty imbalance. We reinterpret these challenges from an embedding geometry perspective, observing that such imbalances induce geometric distortions in hyperspherical representation space. To address this issue, we propose MARGIN (Margin-Aware Regularized Geometry for Imbalanced Vulnerability Detection), a metric-based framework that learns discriminative vulnerability representations through adaptive-margin metric learning and hyperspherical prototype modeling. MARGIN dynamically adjusts geometric regularization according to the distribution structure estimated by the von Mises–Fisher concentration, aligning the probability mass of embedding distributions with their corresponding Voronoi cells, thereby reducing geometric distortion and yielding more stable decision boundaries. Extensive experiments on public vulnerability datasets show that MARGIN consistently outperforms strong baselines, achieving notable improvements in classification and detection, especially on challenging, imbalanced datasets. Further analysis demonstrates that MARGIN produces more structured embedding geometries, improving robustness, interpretability, and generalization.

Index Terms—Software Vulnerability Detection, Software Security, Imbalance Learning, Metric Learning.

I. INTRODUCTION

AS modern software systems keep growing in size and complexity, security vulnerabilities hidden in source code have become a serious threat to software reliability and system safety. These vulnerabilities can cause unexpected program failures or be exploited by attackers to break into systems. Therefore, automatically detecting and classifying vulnerabilities from source code has become an important problem in software engineering.

Recent advances in deep learning have significantly improved software vulnerability detection and classification. However, despite these advances, these models still face substantial challenges when applied to real-world vulnerability datasets. Deep learning-based vulnerability analysis aims to learn discriminative class representations by clustering samples of the same category while separating different categories. However, real-world vulnerability data are often highly imbalanced in both class frequency and sample difficulty, which can bias model optimization, hinder reliable convergence, and degrade generalization performance.

Yuteng Zhang, Huifang Ma, Jiahui Wei, Yafei Yang, and Qingqing Li are with the College of Artificial Intelligence and Computer Science, Northwest Normal University, Lanzhou 730070, China.

Corresponding author: Huifang Ma (email: mahuifang@nwnu.edu.cn).

Manuscript created May, 2026;

Frequency Imbalance. A key challenge in deep learning for vulnerability detection is the severe *frequency imbalance* in real-world software data. This issue appears not only as the imbalance between vulnerable and non-vulnerable code, but more importantly as the uneven distribution across different *Common Weakness Enumeration (CWE)* categories.

As shown in Fig. 1, which presents the frequencies of the top 25 CWE types from recent CVE records (2023–2025), the data follows a clear long-tailed distribution with large differences in sample counts. A small number of common categories, such as CWE-79 (Cross-Site Scripting) and CWE-89 (SQL Injection), contain tens of thousands of samples and make up a large portion of the dataset. In contrast, many other vulnerabilities, such as CWE-400 (Uncontrolled Resource Consumption), CWE-98 (Use of an Improperly Restricted Directory), and CWE-863 (Incorrect Authorization), appear very rarely and only account for a small part of the data.

This large gap in frequency leads to biased metric learning. Standard loss functions like Cross-Entropy and contrastive Loss treat all samples equally [1], so classes with more samples contribute much more to the gradients and dominate the parameter updates. Meanwhile, minority classes provide much weaker signals and have limited influence on the learned representations. In the learned embedding space, majority-class samples typically cluster tightly, while minority-class samples remain scattered and fail to reliably converge around their prototypes. As illustrated in Fig. 3 (a), even when class difficulty is similar, the embeddings of minority class a shows a more dispersed and blur distribution than class b .

Because of this, the model tends to learn biased patterns from high-frequency classes, shifting the decision boundary toward dominant categories while overlooking the subtle characteristics of rare vulnerabilities [2], [3]. Such bias severely limits the reliability of vulnerability detection systems in real-world security scenarios, where accurately identifying rare yet critical vulnerabilities is particularly important.

Difficulty imbalance. Most existing methods for handling imbalanced vulnerability detection primarily focus on frequency imbalance. Common solutions include resampling, cost-sensitive learning, focal loss, and class-balanced reweighting [1], [4]. While these approaches mitigate the influence of majority classes, they usually assume that all classes are equally difficult to learn. Difficulty imbalance can significantly hinder model performance even when class frequencies are balanced, leading to slower convergence, lower precision for difficult classes, and biased evaluation metrics in real-world vulnerability datasets.

In practice, vulnerability datasets also exhibit clear differ-

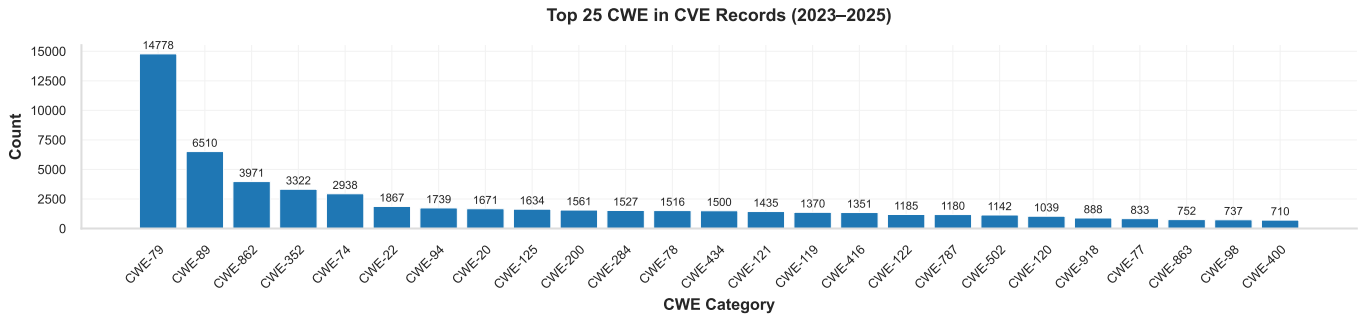


Fig. 1. **Top 25 CWE Types in CVE Project (2023–2025)**. Frequency distribution of CWE categories in publicly disclosed vulnerabilities from the CVE Project. The distribution is highly imbalanced, where a small number of CWE types account for a large portion of vulnerabilities while many others appear only rarely. This long-tailed pattern reflects the uneven real-world occurrence of software weaknesses and highlights the inherent class imbalance in vulnerability datasets.

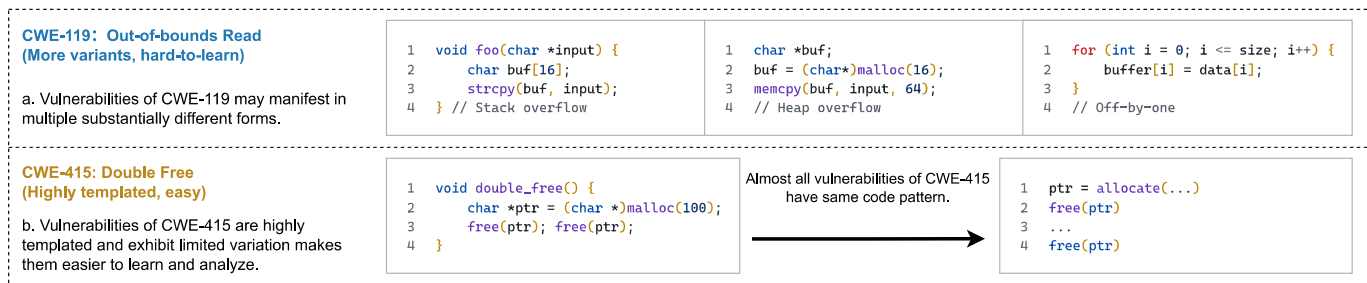


Fig. 2. **Illustration of vulnerability diversity and learning difficulty across two CWE types.** (a) CWE-119 exhibits high embeddings variance with diverse patterns, including stack overflows, heap overflows, and off-by-one errors. (b) In contrast, CWE-415 follows a highly templated `allocate→free→free` pattern with limited variation.

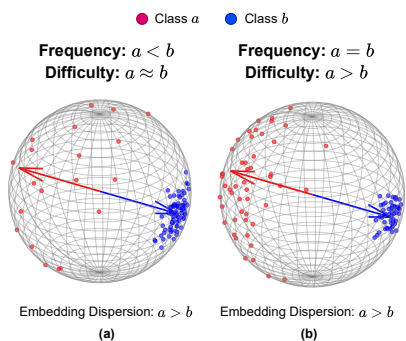


Fig. 3. (a) With comparable class difficulty, lower-frequency classes yield embeddings that are harder to converge around their prototypes on the manifold. (b) With equal class frequencies, higher difficulty (i.e., greater intra-class variance) results in embeddings that are harder to converge around their prototypes on the manifold.

ences in learning difficulty across CWE categories [5]. Although CWE defines a standardized taxonomy, vulnerabilities within the same CWE can vary significantly in syntax, control flow, data flow, and usage context [6], leading to diverse implementation patterns and semantic meanings. As a result, the features extracted by the backbone network from the same class can be highly heterogeneous, especially for difficult classes, where more diverse patterns generate more varied feature vectors, increasing intra-class variance and reflecting higher learning difficulty.

For example, as shown in Fig. 2, CWE-119 (Out-of-bounds

Read) can appear as stack overflows, heap overflows, or off-by-one loop errors, exhibiting rich structural diversity. In contrast, CWE-415 (Double Free) often follows simpler and repetitive patterns, where the same pointer is freed multiple times. This suggests that class difficulty is closely related to the diversity of feature representations: classes with higher structural diversity produce more high-variance embeddings from the backbone, complicating optimization and slowing convergence.

In this work, it’s hard to quantify the accurate difficulty directly so we quantify difficulty imbalance by treating intra-class feature variance as a proxy for class difficulty. Prior studies have confirmed that higher intra-class variance correlates with increased learning difficulty [7], reflecting greater dispersion, noise, and inconsistency within class representations—a manifestation of the well-known *Bias–Variance Dilemma*. We attribute this difficulty imbalance to the feature geometry learned by the backbone. Under this setting, difficult classes show high feature variance in the embedding space [3], [8]. Easy classes form compact clusters due to simpler and more consistent patterns, whereas difficult classes remain more dispersed. Their semantic heterogeneity causes the backbone to produce overly dispersed features, destabilizing the decision boundary and hindering convergence—an issue that traditional imbalance learning strategy cannot resolve.

As illustrated in Fig. 3(b), even when class frequencies are identical, the difficult class *a* exhibits a more scattered distribution than class *b*. When frequency imbalance and difficulty imbalance coexist, the learned representations show

varying degrees of compactness across classes [3], both of which can be interpreted geometrically as the concentration of samples around their class prototypes in the embedding space.

Lack of Interpretability. Most existing approaches mainly aim to improve classification performance, while paying less attention to the interpretability. Common evaluation metrics such as MCC and F1-score only reflect prediction results, but cannot show whether the embedding space has clear and well-discriminated geometric structures under severe imbalance [2]. Without explicit constraints on representation geometry, models may depend on locally optimal but unstable decision boundaries, which can be highly sensitive to distribution shifts or rare vulnerability patterns. For security-critical tasks like vulnerability detection, such instability can greatly reduce practical reliability.

In essence, both frequency imbalance and difficulty imbalance can be unifiedly viewed as a shared geometric issue in the embedding space, namely the uneven concentration of class distributions. Our work shows that imbalance in vulnerability detection is closely related to distortion in the learned embedding geometry [3], [4]. Frequency and difficulty imbalance cause dominant classes to have much dispersed and distort distribution in the learned decision space. Therefore, explicitly modeling the embedding space from a geometric and manifold perspective in metric learning offers a more principled way to improve both robustness and interpretability.

To address these challenges, we propose **MARGIN** (**M**argin-**A**ware **R**egularized **G**eometry for **I**mbalanced **V**ulnerability **D**etectio**N**), a metric-based framework that revisits vulnerability detection from a hyperspherical embedding perspective. It provides a unified geometric view in which both frequency and difficulty imbalance are described by how concentrated each class is on the hypersphere. By explicitly shaping the geometry of the embedding space, MARGIN reduces representation bias through adaptive margin learning and prototype-based regularization. This helps stabilize decision boundaries and improves the separation between classes under severe imbalance. Overall, the framework connects practical imbalance handling with a clear geometric interpretation, leading to better performance and improved interpretability.

The contributions of this paper are summarized as follows:

- 1) We revisit two critical imbalances in vulnerability detection, i.e., *frequency imbalance* and *difficulty imbalance*, and analyze their effects in an interpretable manner from the perspective of embedding geometry. (Section III)
- 2) We propose **MARGIN**, a metric-learning framework that integrates adaptive mechanisms and hyperspherical prototype modeling to mitigate both imbalances simultaneously. (Section IV)
- 3) Extensive experiments on multiple public vulnerability datasets demonstrate that MARGIN consistently improves vulnerability detection and classification performance. (Section V, VII)

II. PRELIMINARIES

A. Problem Formulation

We consider a vulnerability dataset $\mathcal{D} = \{(x_i, y_i)\}_{i=1}^N$, where each sample consists of a code snippet $x_i \in \mathcal{X}$ and a class label $y_i \in \mathcal{Y}$. The label space is defined as $\mathcal{Y} = \{\text{Non-Vul}, \text{CWE-a}, \text{CWE-b}, \dots\}$, where **Non-Vul** denotes non-vulnerable code and each **CWE-*** represents a specific vulnerability category defined in the CWE.

This task is formulated as a *single-label multi-class classification* problem in close-set, where each code sample is associated with exactly one label. In practice, real-world datasets exhibit severe frequency and difficulty imbalance across different labels.

B. Cosine Softmax Loss

To address class imbalance in vulnerability detection from a geometric perspective, we adopt a unit hyperspherical prototype-based classification framework. This formulation defines a structured manifold that can be explicitly analyzed and regularized, allowing imbalance to be tackled in a unified geometric manner. Each class is represented by a prototype, serving as a stable and interpretable semantic center in the embedding space [9].

We begin with the standard *Cosine Softmax Loss* for single-label multi-class classification. For each input, the encoder produces a d -dimensional feature, and we apply ℓ_2 normalization to both the feature $\mathbf{e} \in \mathbb{R}^d$ and classifier weight $\mathbf{w}_i \in \mathbb{R}^d$. The linear classifier then produces logits for each class, followed by the standard softmax cross-entropy loss:

$$z_i = \tilde{\mathbf{w}}_i^\top \tilde{\mathbf{e}}, \quad \ell_i = -\log \frac{\exp(z_i)}{\sum_{j=1}^{|\mathcal{Y}|} \exp(z_j)}, \quad i \in \mathcal{Y} \quad (1)$$

The logit z_i can be also decomposed as:

$$z_i = \cos \theta_i \quad (2)$$

where θ_i denotes the angle between $\tilde{\mathbf{w}}_i$ and $\tilde{\mathbf{e}}$. Thus, the decision score depends purely on angular similarity and vector magnitude variations are eliminated.

We introduce the scaling factor s_0 to sharpen the logits and the resulting cosine softmax loss is defined as:

$$\ell_i = -\log \frac{\exp(s_0 \cos \theta_i)}{\sum_{j=1}^{|\mathcal{Y}|} \exp(s_0 \cos \theta_j)} \quad (3)$$

The cosine softmax loss makes both features and class weights lie on the unit hypersphere \mathbb{S}^{d-1} . We interpret $\tilde{\mathbf{w}}_i$ as the *Weight Prototype* of class i . Training therefore encourages samples to align with their corresponding prototypes, forming compact clusters separated by angular margins. This geometric view enables explicit analysis of imbalance effects in embedding space.

C. Voronoi Cell and Neural Collapse

Recent studies show that deep classifiers without prediction bias and trained on ideal balanced data tend to exhibit the Equiangular Tight Frame (ETF) structure under *Neural Collapse* phenomenon during the later stage of training [10], all weight prototypes converge to a highly symmetric geometric configuration: the pairwise similarity between weight prototypes converge to a constant, resulting in prototypes that are uniformly distributed on the unit hypersphere:

$$\tilde{\mathbf{w}}_i^\top \tilde{\mathbf{w}}_j = -\frac{1}{|\mathcal{Y}| - 1}, \quad \forall i \neq j \quad (4)$$

In this setting, the unit hypersphere \mathbb{S}^{d-1} can be partitioned into $|\mathcal{Y}|$ spherical regions centered around each weight prototype, where all regions are of equal size. These regions correspond to the *Voronoi Cells*. When the number of classes $|\mathcal{Y}|$ is sufficiently large, the shape of each Voronoi cell approaches a spherical cap on the hypersphere. Taking each Voronoi cell as the base and the center of the unit hypersphere as the apex, we obtain a cone whose base is the corresponding Voronoi cell. We have the apex angle of hyperspherical cone which base is Voronoi cell, referred as *Voronoi Apex Angle*:

$$\theta^{\text{cell}} = \arccos\left(-\frac{1}{|\mathcal{Y}| - 1}\right) \quad (5)$$

We also refer the hyperspherical cone as the *Voronoi Cone*.

At the same time, the probability mass regions of embeddings for each class converge to be equal in size and lie predominantly within the corresponding Voronoi cell defined by its weight prototype. Also, the mean feature prototype of each class aligns with its corresponding weight prototype. Let $\tilde{\boldsymbol{\mu}}_i$ denote the normalized mean feature of class i . Under Neural Collapse, we have $\tilde{\boldsymbol{\mu}}_i = \tilde{\mathbf{w}}_i$, for all $i \in 1, \dots, |\mathcal{Y}|$.

Ideally, the ETF structure yields clearly discriminative and unbiased decision boundaries [3]. However, under class-imbalanced conditions, such an ETF structure cannot be properly established, resulting in geometrically less separable representations, which in turn gives rise to the distortion region. This observation suggests that, to alleviate the prediction bias induced by class imbalance from a geometric perspective, it is essential to explicitly encourage the embedding distribution to evolve toward an ETF structure.

D. vMF Distribution for Hyperspherical Modeling

Following the principle of maximum entropy, feature embeddings are represented on the unit hypersphere. The von Mises–Fisher (vMF) distribution is employed as a quantitative tool to characterize class-wise feature concentration. In this framework, the concentration parameter κ_i measures how tightly samples cluster around their mean direction $\boldsymbol{\mu}_i$ [11]. Formally, a normalized embedding $\tilde{\mathbf{e}} \in \mathbb{S}^{d-1}$ follows a vMF distribution $\tilde{\mathbf{e}} \sim \text{vMF}(\tilde{\boldsymbol{\mu}}_i, \kappa_i)$ if

$$p(\tilde{\mathbf{e}} | \tilde{\boldsymbol{\mu}}_i, \kappa_i) = C_d(\kappa_i) \exp\left(\kappa_i \tilde{\boldsymbol{\mu}}_i^\top \tilde{\mathbf{e}}\right) \quad (6)$$

where

$$C_d(\kappa_i) = \frac{\kappa_i^{\frac{d}{2}-1}}{(2\pi)^{\frac{d}{2}} I_{\frac{d}{2}-1}(\kappa_i)} \quad (7)$$

and $I_\nu(\cdot)$ denotes the modified Bessel function of the first kind.

A larger κ_i indicates stronger concentration of embeddings around $\tilde{\boldsymbol{\mu}}_i$, leading to more compact class distributions.

Under the vMF assumption, the high-density region of each class on the hypersphere can be approximated as a spherical cap centered at $\tilde{\boldsymbol{\mu}}_i$. Taking this region as the base and the center of the unit hypersphere as the apex, we obtain a hyperspherical cone, refer as the *vMF Confidence Cone*.

For a given confidence level α , the corresponding high-probability region satisfies

$$P\left(\arccos(\tilde{\boldsymbol{\mu}}_i^\top \tilde{\mathbf{e}}) \leq \theta_i^{\text{vMF}}\right) = \alpha \quad (8)$$

where θ_i^{vMF} denotes the apex angle of the hyperspherical cone induced by the vMF distribution. This angle is also referred to as the *vMF Apex Angle*.

Importantly, for a fixed confidence level α , the apex angle θ_i^{vMF} is solely determined by the concentration parameter κ_i . A larger κ_i leads to a smaller apex angle, indicating tighter concentration around the prototype, whereas a smaller κ_i produces a wider apex angle, reflecting more dispersed intra-class distributions.

III. MOTIVATION ANALYSIS

Under the dual imbalance of class frequency and difficulty, neural networks in the late training stage—upon reaching the Neural Collapse regime—learn hyperspherical embeddings where class prototypes are well separated with large angular distances. As illustrated in Fig. 4, let P_a and P_b denote the prototypes of classes a and b , respectively.

According to the argmax decision rule, the angular bisectors of $\angle P_a O P_b$ and $\angle P_b O P_a$, denoted as OQ_1 and OQ_2 , partition the unit hypersphere into regions with equal angular boundaries. These regions define the *Voronoi cells* of classes a and b , namely $\widehat{Q_1 P_a Q_2}$ and $\widehat{Q_1 P_b Q_2}$, each with a fixed apex angle θ^{cell} . The Voronoi cells therefore act as ideal decision regions.

However, under imbalance, class-conditional embeddings do not always concentrate tightly around their corresponding prototypes. Instead, they may deviate and extend beyond their associated Voronoi cells, leading to misclassification [3].

To characterize this phenomenon, consider the binary classification scenario shown in Fig. 4. The embeddings of classes a and b can be reasonably approximated as following vMF distributions on \mathbb{S}^1 . Their probability mass regions can be viewed as spherical caps, namely $\widehat{A_1 O A_2}$ and $\widehat{B_1 O B_2}$, with vMF apex angles θ_a^{vMF} and θ_b^{vMF} , where typically $\theta_a^{\text{vMF}} > \theta_b^{\text{vMF}}$. This indicates that class a exhibits a more dispersed embedding distribution.

Crucially, these probability mass regions may exceed their corresponding Voronoi cells, i.e., $\theta_a^{\text{vMF}} > \theta^{\text{cell}}$, $\theta_b^{\text{vMF}} > \theta^{\text{cell}}$. For class a , the exceeding portions $\widehat{Q_1 O A_1}$ and $\widehat{Q_2 O A_2}$ intrude into the Voronoi cell $\widehat{Q_1 P_b Q_2}$ of class b , leading to false

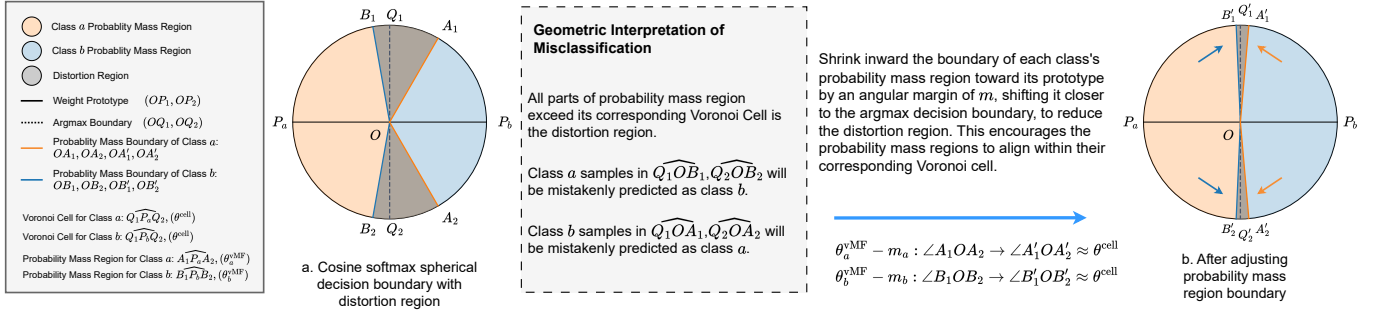


Fig. 4. **Geometric Interpretation of Misclassification and Heuristic Design of MARGIN** Conceptual illustration of spherical angular spans for class decision of Cosine Softmax Loss and MARGIN on \mathbb{S}^1 .

negatives for class a and false positives for class b . Similar phenomenon applies to class b .

We define the union of all such probability masses that lie outside its corresponding Voronoi cell and enter those of other classes as the *distortion region*, specifically $\widehat{A_1OB_1}$ and $\widehat{A_2OB_2}$. This distortion region reflects the geometric mismatch between class-conditional embedding distributions and Voronoi decision regions, and directly leads to misclassification and prediction bias under dual imbalance that causes increment of FPR and FNR.

Therefore, the core challenge is not merely the class imbalance itself, but the misalignment between the geometry of embedding distributions and the induced decision regions. An effective learning strategy should explicitly constrain the embedding distribution to reduce the distortion region.

To this end, we introduce a margin constraint into the cosine softmax loss, enforcing that each sample of class i remains within an angular distance m_i from its corresponding prototype. This imposes an upper bound on the angular support of the class-conditional distribution, effectively contracting its probability mass region (i.e., reducing θ_i^{vMF}). As a result, intra-class embeddings become more compact and better aligned with their Voronoi cells, thereby mitigating the distortion region.

However, a fixed margin contradicts the heterogeneous dispersion induced by dual imbalance (e.g., $\theta_a^{\text{vMF}} > \theta_b^{\text{vMF}}$). Classes with highly dispersed probability mass region require stronger constraints to sharpen decision boundary, while more concentrated classes benefit from loose margins to maintain stable optimization. This reveals a fundamental limitation of static margin designs [12].

To address this, we propose a dynamic margin mechanism that adapts m_i according to the geometric structure of each class during training. By explicitly modeling class-conditional distributions on the hypersphere and adjusting margins based on their concentration, our approach aims to align the probability mass region (e.g., $\widehat{A_1OA_2}$) with its corresponding Voronoi cell (e.g., $\widehat{Q_1P_aQ_2}$), thereby minimizing the distortion region.

IV. METHODOLOGY

A. Feature Extraction and Normalization

Given a code sample \mathcal{X} , we employ CodeT5 as the transformer backbone to extract a 768-dimensional semantic vector

$e_i \in \mathbb{R}^{768}$ from the final [CLS] token. While MARGIN is backbone-agnostic, we adopt CodeT5 due to its widespread adoption in code representation tasks. This choice ensures that observed performance gains are attributable to MARGIN rather than the backbone, as confirmed by our ablation studies; preliminary experiments with alternative encoders, such as CodeBERT and GraphCodeBERT, yield consistent improvements, further validating the method's backbone-independent nature. To enforce a geometrically interpretable space, we apply ℓ_2 -normalization to both feature embeddings and classifier prototypes.

B. Approximation of Kappas

To quantify each class's concentration on the hypersphere, we estimate the vMF parameter κ_i via Maximum Likelihood Estimation (MLE). Given the normalized embeddings of class i , we first compute the mean resultant length from the empirical mean vector.

The MLE of κ_i involves a ratio of modified Bessel functions, which has no closed-form inverse and usually requires iterative optimization. To simplify, we use the high-dimensional approximation of Banerjee et al. [11].

$$\kappa_i \approx \frac{\|\boldsymbol{\mu}_i\|(d - \boldsymbol{\mu}_i^2)}{1 - \boldsymbol{\mu}_i^2} \quad (9)$$

Here, d is the embedding dimensionality. The approximation is accurate in high dimensions; with CodeT5 producing 768-dimensional embeddings, it is both empirically justified and widely used in prior work.

C. Align vMF Apex Angle with Voronoi Apex Angle

To characterize the angular uncertainty of each class on the hypersphere, we estimate the vMF Apex Angle for each class based on its underlying vMF distribution.

On the unit hypersphere, the confidence level α under a vMF distribution for class i satisfies

$$\alpha = \frac{\int_0^{\theta_i^{\text{vMF}}} (\sin \theta)^{d-2} e^{\kappa \cos \theta} d\theta}{\int_0^\pi (\sin \theta)^{d-2} e^{\kappa \cos \theta} d\theta} \quad (10)$$

In practice, we set $\alpha = 95\%$, and the corresponding vMF apex angle is given by

$$\theta_i^{\text{vMF}} = \arccos(F_i^{-1}(1 - \alpha)) \quad (11)$$

where F_i^{-1} denotes the inverse marginal cumulative distribution function of the vMF distribution for class i . Since no closed-form solution exists, we adopt an efficient approximation. Given the concentration parameter κ_i of class i , we define the effective concentration as κ_i .

Based on the effective concentration, the apex angle of the vMF confidence cone is approximated as

$$\theta_i^{\text{vMF}} = \sqrt{\frac{\chi_\alpha^2(d-1)}{\kappa_i}} \quad (12)$$

where $\chi_\alpha^2(d-1)$ denotes the α -quantile of the chi-square distribution with $d-1$ degrees of freedom. This follows from the asymptotic property of vMF distributions that, under high concentration, local angular deviations can be approximated by a Gaussian distribution on the tangent space [8], [13].

To constrain each class probability mass region within its Voronoi cell, we align the vMF apex angle with the Voronoi apex angle via an adaptive angular margin. Considering the symmetry of the hyperspherical cone angle, we divide it by two to define the margin with Non-negativity constraint:

$$m_i = \max\left(\frac{\theta_i^{\text{vMF}} - \theta^{\text{cell}}}{2}, 0\right) \quad (13)$$

However, in the later stages of training, even when θ_i^{vMF} is aligned with θ^{cell} , the Voronoi cell is not a perfect hyperspherical circle that covers the vMF probability mass region, in order to maintain strong regularization and further enhance training, we need to continue aligning it with the smallest vMF apex angle $\theta_{\min}^{\text{vMF}}$. It serves to maintain compactness of class embeddings even after the vMF confidence cone has aligned with the Voronoi cone. This prevents late-stage relaxation of the embedding space and stabilizes prototype-based classification. Therefore, we have:

$$m_i = \max\left(\frac{\theta_i^{\text{vMF}} - \theta^{\text{cell}}}{2}, \frac{\theta_i^{\text{vMF}} - \theta_{\min}^{\text{vMF}}}{2}\right) \quad (14)$$

When the vMF confidence cone exceeds the Voronoi boundary, the excess region indicates potential inter-class overlap. The adaptive margin therefore penalizes excessive dispersion beyond the Voronoi partition, improving hyperspherical separability and reducing class interference.

D. Concentration-Aware Logits Scaling

To adapt classifier confidence to class compactness, we adjust the logit scaling factors according to the convergence status of each class.

The concentration parameter κ_i reflects the compactness of class representations on the hypersphere. A larger κ_i indicates that class i is well optimized with low intra-class variance; assigning large logits in this case may lead to over-confident predictions and dominate gradient updates. Therefore, we assign smaller scaling factors to such classes to suppress their influence. In contrast, a smaller κ_i indicates a more

dispersed distribution and insufficient convergence, for which we increase the scaling factors to sharpen logits and amplify gradient signals.

To achieve this behavior while avoiding the instability of explicit inverse mappings, we adopt a *soft ranking-based strategy* in the log-concentration space. Specifically, we compute:

$$r_i = |\mathcal{Y}| \cdot \text{softmax}\left(\frac{\log \kappa_i}{|\mathcal{Y}|}\right) \quad (15)$$

where C is the number of classes, ensuring $r_i > 0$ and unit mean.

We then reverse the allocation order according to the ranking of κ_i , assigning larger weights to lower-concentration classes:

$$\tilde{r} = \text{Reverse}(r) \quad (16)$$

Finally, the class-wise scaling factors are:

$$s_i = s_0 \cdot \tilde{r}_i \quad (17)$$

where s_0 is a base scaling factor.

This formulation enables geometry-aware and difficulty-adaptive gradient reallocation, enhancing under-converged classes while preventing well-optimized ones from dominating training.

E. Objective Function

The resulting difficulty and frequency-aware kappa loss with adaptive margin and scaling factor for a sample of class i is:

$$l_i = -\log \frac{\exp(s_i \cos(\theta_i + m_i))}{\exp(s_i \cos(\theta_i + m_i)) + \sum_{j \neq i} \exp(s_j \cos \theta_j)} \quad (18)$$

F. Inference on Test

Instead of directly using classifier weights as prototypes, on evaluation stage, we construct data-driven prototypes from training embeddings to better capture the empirical geometry of the feature space. Specifically, for each class $i \in \mathcal{Y}$, we compute the geometric median of its normalized training embeddings and project it onto the unit hypersphere:

$$\mathbf{p}_i = \arg \min_{\mathbf{p}} \sum_{x_i \in \mathcal{D}_i} \|\mathbf{p} - \tilde{\mathbf{e}}_i\|_2, \quad \tilde{\mathbf{p}}_i = \frac{\mathbf{p}_i}{\|\mathbf{p}_i\|_2} \quad (19)$$

Compared to weight-based prototypes, geometric medians are more robust to outliers and better reflect class-wise embedding distributions.

Inference is performed via nearest-prototype matching in angular space:

$$\hat{y} = \arg \max_{y \in \mathcal{Y}} \tilde{\mathbf{e}}_{\text{test}}^\top \tilde{\mathbf{p}}_i \quad (20)$$

This induces a Voronoi partition on \mathbb{S}^{d-1} , where each sample is assigned to the angular region of its closest prototype.

TABLE I
STATISTICS OF VULNERABILITY DETECTION DATASETS.

Dataset	Amount	Vul/Non-Vul IR	CWEs	Labels CV
BigVul	43184	18.57	10	3.13
MegaVul	147423	18.55	15	3.78
ReposVul	82037	31.17	13	3.61

V. EXPERIMENTS

All experiments were conducted on a single NVIDIA RTX5880 Ada (48 GB) with CUDA 12.4. All methods were evaluated under identical settings unless otherwise specified. In both the baseline and ablation experiments, to validate the effectiveness of our method and mitigate random fluctuations, we conducted each experiment five times with different random seeds. To comprehensively evaluate the effectiveness of MARGIN, we design the following research questions:

- **RQ1:** How effective is the proposed method compared with baseline approaches?
- **RQ2:** How do the proposed adaptive mechanisms contribute to performance?
- **RQ3:** How sensitive is MARGIN to different hyperparameter settings?
- **RQ4:** How much time does MARGIN take?

A. Datasets

We evaluate MARGIN on three widely used public vulnerability detection datasets: **BigVul** [14], **MegaVul** [15], and **ReposVul** [16]. These datasets, collected from open-source repositories, CVE/NVD reports, and vulnerability-fixing commits, vary in scale and CWE distribution, and are highly imbalanced, with non-vulnerable samples dominating, providing realistic benchmarks for imbalanced vulnerability detection.

BigVul and MegaVul are large-scale C/C++ datasets, while ReposVul emphasizes higher data quality through automated vulnerability disentanglement and dependency-aware filtering.

Following prior work, we perform standard preprocessing, to obtain stable and reliable data splits, we further select approximately the top 10-15 most frequent CWE categories while preserving the original long-tailed distribution [5]. This ensures sufficient samples per class for training and evaluation while preserving the original long-tailed characteristics of the data distribution. All datasets are split into training, validation, and test sets with a ratio of 8:1:1.

B. Baselines

To comprehensively evaluate the effectiveness of MARGIN for CWE-based single-label multi-class vulnerability classification, we compare our method against representative baselines from three categories, including graph-based methods, program analysis-based approaches, and recent representation learning models. Specifically, the compared baselines include **ReVeal**(2021, TSE) [17] and **LIVABLE**(2024, TSE) [18], which leverage graph neural networks for structural vulnerability modeling; **μ VulDeePecker**(2021, DSC) [19] and **SySeVR**(2022, DSC) [20], which exploit vulnerability-aware

program analysis and code slicing; and **HCL-VC**(2024, EMNLP) [21], **MoEVD**(2025, FSE) [22], and **CLeVeR**(2025, ACL) [23], which represent recent advances in CWE-aware representation learning and vulnerability classification. For fair comparison, we follow the hyperparameter settings recommended in the original papers. When official implementations are unavailable, models are reproduced based on publicly released code or reported configurations.

C. Metrics

We evaluate MARGIN from two complementary perspectives: (i) **Binary Vulnerability Detection** and (ii) **Fine-grained CWE Classification**. Given the severe class imbalance, we adopt imbalance-robust metrics.

For binary detection, we collapse all CWE categories into a single positive class (*Vulnerable*) and treat *Non-Vul* as the negative class. We report Precision, Recall, F1-score, and Matthews Correlation Coefficient (MCC).

For multi-CWE classification, we follow a one-vs-all (OvA) scheme over all classes to compute per-class Precision, Recall, F1-score, and MCC. To specifically assess vulnerability-type recognition, we exclude the *Non-Vul* class and compute macro-averaged metrics over all CWE classes, referred to as **CWE-Macro** metrics.

VI. DISCUSSION

A. Overall Performance Comparison (RQ1)

Across BigVul, MegaVul, and ReposVul, MARGIN consistently outperforms most baselines in both vulnerability detection and CWE classification, with clear gains in F1 score (Table II).

On BigVul, MARGIN achieves the best binary F1 (**86.57%**) and MCC (**85.88%**), surpassing HCL-VC. For CWE classification, it reaches a macro-F1 of **70.72%** and macro-precision of **73.35%**, outperforming CLeVeR by over 7 points, showing strong performance in both detection and fine-grained classification.

On the more challenging MegaVul dataset, MARGIN still performs best, with a binary F1 of **51.06%** and a high precision of **66.66%**, indicating fewer false positives under severe class imbalance. It also achieves a macro-F1 of **34.65%**, improving over LIVABLE (**32.68%**), showing more reliable CWE predictions.

On ReposVul, which reflects real-world scenarios, MARGIN achieves a binary F1 of **43.85%**, higher than μ VulDeePecker (**42.01%**). For CWE classification, it obtains the best macro-F1 (**34.39%**) and macro-recall (**48.60%**), showing good generalization.

Other sequence-based methods (e.g., SySeVR, μ VulDeePecker) generally achieve high recall but low precision, resulting in more false positives. Structure-aware methods (e.g., HCL-VC, LIVABLE, CLeVeR) are more balanced but underperform on rare CWE types. MARGIN improves the recall-precision balance and boosts performance on rare classes.

Statistical tests confirm consistent macro-F1 gains ($p < 0.05$ in most cases). For binary F1, MARGIN clearly outperforms

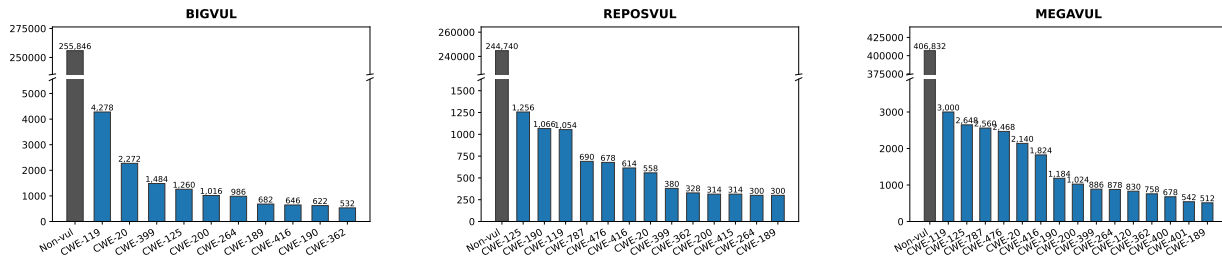


Fig. 5. **Classes distribution across labels.** In terms of frequency, non-vulnerable samples dominate the gaps, while the remaining CWE vulnerability samples exhibit a long-tailed distribution. Overall, the label distribution is highly imbalanced.

traditional methods, while differences with recent strong baselines are often insignificant, likely due to near-saturation.

Overall, MARGIN mainly improves feature representation, leading to better class-level discrimination rather than just higher overall accuracy. These results confirm its effectiveness, especially for imbalanced data and real-world vulnerability analysis.

B. Contribution of Adaptive Mechanisms (RQ2)

To investigate the impact of the adaptive mechanisms in MARGIN, we conducted ablation studies by selectively removing each key component. Table III summarizes the performance results.

Removing the adaptive margin significantly affects the binary detection recall, which increases to **87.66%** while precision drops to **82.97%**, indicating a shift in the decision boundary that favors sensitivity over specificity. For vulnerability classification, the macro-MCC and macro-F1 decrease compared to the full model, highlighting that the adaptive margin contributes to balanced performance across classes by properly calibrating inter-class margins.

Disabling the adaptive logits scaling slightly improves binary MCC and F1, but the recall decreases to **85.05%** and precision drops to **89.60%**, suggesting a less robust separation in the feature space. For classification, the macro-MCC and macro-F1 also drop compared to the full model, confirming that the scaling factor helps stabilize the learning dynamics and enhances discriminative power for minority classes.

The full model consistently achieves the best performance. In binary detection, it attains a high F1 of **87.47%** with balanced recall and precision. For classification, it achieves the highest macro-MCC (**71.29%**) and macro-F1 (**71.13%**), showing that combining both adaptive mechanisms improves detection and classification, especially for rare CWE types. Ablation results also confirm that removing geometric constraints causes a significant drop even with CodeT5 fixed, indicating the gains stem from the geometric constraints rather than the feature extractor.

In summary, ablation results confirm that both the adaptive margin and logits scaling are crucial for MARGIN, with the margin calibrating inter-class distances and the scaling factor stabilizing training and enhancing discriminability.

C. Hyperparameter Sensitivity Analysis (RQ3)

Despite incorporating adaptive margins and class-specific adjustments, MARGIN introduces only a single explicit hyperparameter, the base scaling factor s_0 , which controls the magnitude of geometric modulation in the hyperspherical feature space.

We evaluate its sensitivity on BigVul (Table IV). The best binary F1 (**87.35%**) and macro-MCC (**71.22%**) are achieved at $s_0 = 20$, with stable performance observed for $s_0 \in [15, 25]$. Smaller values (e.g., $s_0 = 10$) reduce inter-class separation, lowering macro-MCC to **63.78%**, while excessively large values (e.g., $s_0 = 60$) decrease binary F1 to **85.00%** due to over-confident margins.

The trend is non-monotonic: increasing s_0 initially improves both detection and classification, but beyond $s_0 \approx 30$, metrics may fluctuate. This reflects a trade-off in modulating hyperspherical decision boundaries: moderate scaling promotes well-separated and stable boundaries, while extreme values can reduce robustness.

The optimal s_0 varies across datasets. Empirically, noisier or intrinsically harder datasets benefit from slightly larger s_0 to strengthen gradients and sharpen boundaries, whereas cleaner or easier datasets favor smaller s_0 to prevent overconfident predictions. These insights offer practical guidance for tuning s_0 .

D. Computation Costs of MARGIN (RQ4)

Due to differences in hardware, pretraining strategies, implementation, and data preprocessing, direct efficiency comparisons with prior work may be unfair. We therefore report only the efficiency of the proposed method.

We adopt the approximation of kappa given in equation 9, which has constant time complexity and incurs no additional computational overhead. In addition, computing class prototypes using the Weiszfeld algorithm in fixed dimension d has linear time complexity $O(n)$, which matches the per-iteration complexity of training. Therefore, the prototype computation does not increase the overall time complexity or delay convergence, and is considered acceptable for practical use.

MARGIN’s computational cost in training and inference is largely determined by the backbone encoder. The adaptive margin and scaling factor mechanisms introduce additional constraints, which empirically improve gradient signals and accelerate convergence. Using CodeT5 as the backbone, average training latency is **167–200 ms** per sample, and inference

TABLE II
BASELINE COMPARISON. p -VALUES ARE COMPUTED ON F1 SCORES USING T-TEST AGAINST MARGIN.

Dataset	Method	Vulnerability Detection Performance (Vul/Non-vul Binary)				Vulnerability Classification (CWE-Macro)			
		MCC(%)	F1(%) (p -value)	Recall(%)	Precision(%)	Macro-MCC(%)	Macro-F1(%) (p -value)	Macro-R(%)	Macro-P(%)
BIGVUL	SySeVR	65.54±2.1	63.94±1.8 (1.6e-06)	95.36±2.8	48.10±1.5	44.03±1.2	42.61±1.1 (2.6e-08)	52.39±1.4	42.28±1.3
	μ VulDeePecker	69.30±2.3	68.58±2.2 (5.2e-06)	93.61±3.1	54.11±1.8	41.53±1.1	39.54±1.0 (2.5e-08)	42.91±1.2	46.61±1.4
	ReVeal	78.88±2.5	79.74±2.5 (3.7e-03)	87.37±2.9	73.33±2.4	25.06±0.8	21.76±0.7 (1.9e-08)	30.88±0.9	34.31±1.1
	LIVABLE	83.69±2.7	84.48±2.7 (2.6e-01)	88.10±2.9	81.15±2.7	61.91±1.6	60.86±1.5 (1.7e-05)	60.87±1.6	65.95±2.0
	HCL-VC	84.64±2.8	85.42±2.8 (5.3e-01)	85.05±2.8	85.80±2.8	66.37±1.7	66.17±1.7 (3.4e-03)	68.62±1.8	65.17±2.0
	MoEVD	81.84±2.6	82.74±2.6 (5.5e-02)	85.92±2.8	79.78±2.6	34.99±0.9	33.93±0.9 (1.9e-08)	38.40±1.0	35.24±1.1
	CLeVeR	84.30±2.7	85.06±2.7 (4.1e-01)	88.82±2.9	81.60±2.7	64.09±1.6	63.76±1.6 (2.1e-04)	66.11±1.7	63.48±2.0
	MARGIN	85.88±2.8	86.57±2.8 (-)	88.00±2.9	85.19±2.8	70.91±1.8	70.72±1.8 (-)	69.47±1.8	73.35±2.2
MEGAVUL	SySeVR	27.32±1.8	24.30±1.6 (4.7e-06)	84.78±6.6	14.19±0.9	12.24±0.8	9.53±0.6 (6.3e-06)	30.73±2.0	6.37±0.4
	μ VulDeePecker	25.02±1.6	22.94±1.5 (4.5e-06)	80.58±6.3	13.37±0.9	6.56±0.4	5.35±0.4 (5.6e-06)	16.55±1.1	4.95±0.3
	ReVeal	32.80±2.1	31.88±2.1 (1.5e-05)	72.84±5.7	20.40±1.3	17.42±1.1	15.17±1.0 (5.5e-06)	32.21±2.1	10.97±0.7
	LIVABLE	47.49±3.5	50.18±3.4 (6.9e-01)	50.32±3.3	50.05±3.3	32.80±2.2	32.68±2.2 (2.0e-01)	32.00±2.1	34.74±2.3
	HCL-VC	43.06±1.4	45.64±3.0 (2.7e-02)	56.97±3.7	38.06±2.5	25.74±1.7	25.20±1.7 (1.2e-04)	30.71±2.0	23.15±1.5
	MoEVD	46.53±3.0	49.31±3.2 (4.2e-01)	50.32±3.8	48.34±3.2	28.98±1.9	28.85±1.9 (2.7e-03)	29.44±1.9	29.76±2.0
	CLeVeR	48.25±3.2	50.82±1.6 (8.9e-01)	49.59±3.5	52.11±3.4	30.43±2.0	30.21±2.0 (1.2e-02)	29.57±1.9	32.67±2.2
	MARGIN	50.59±3.3	51.06±3.3 (-)	41.38±2.7	66.66±4.4	35.95±2.4	34.65±2.3 (-)	20.00±1.3	47.36±3.1
REPOSVUL	SySeVR	22.03±1.4	16.77±1.1 (6.0e-07)	82.19±4.2	9.34±0.6	19.31±1.0	13.72±0.7 (1.7e-06)	53.71±2.7	8.62±0.4
	μ VulDeePecker	40.50±2.1	42.01±2.1 (2.2e-01)	51.15±2.6	35.64±1.8	31.46±1.6	30.84±1.5 (1.0e-02)	36.99±1.9	28.02±1.4
	ReVeal	38.69±2.0	39.88±2.0 (2.0e-02)	52.42±2.7	32.19±1.6	32.13±1.6	31.29±1.6 (2.1e-02)	39.15±2.0	27.76±1.4
	LIVABLE	37.15±1.9	37.90±1.9 (2.3e-03)	54.20±2.8	29.14±1.5	31.20±1.6	29.80±1.5 (2.5e-03)	41.48±2.1	25.15±1.3
	HCL-VC	34.71±1.8	33.85±1.7 (8.1e-05)	60.81±3.1	23.45±1.2	30.74±1.6	28.56±1.5 (6.0e-04)	44.65±2.3	24.12±1.2
	MoEVD	41.05±2.1	42.66±2.2 (4.3e-01)	39.95±2.0	45.77±2.4	29.80±1.5	29.59±1.5 (2.0e-03)	28.03±1.4	32.62±1.7
	CLeVeR	38.95±2.0	40.24±2.1 (3.2e-02)	51.91±2.7	32.85±1.7	32.31±1.6	31.47±1.6 (2.7e-02)	40.16±2.1	27.15±1.4
	MARGIN	42.08±2.2	43.85±2.3 (-)	48.60±2.5	39.95±2.1	34.80±1.8	34.39±1.8 (-)	48.60±2.5	39.95±2.1

TABLE III
ABLATION STUDY OF KEY COMPONENTS IN MARGIN(CODET5 AS BACKBONE).

Variant	Vulnerability Detection (Vul/Non-vul Binary)				Vulnerability Classification (CWE-Macro)			
	MCC(%)	F1(%)	R(%)	P(%)	Macro-MCC(%)	Macro-F1(%)	Macro-R(%)	Macro-P(%)
Cosine Softmax Only	85.94±2.6	86.56±2.7	83.16±3.2	90.24±2.4	64.03±2.0	63.78±2.1	60.67±2.5	68.57±2.2
w/o Adaptive Margin	84.47±2.8	85.25±2.9	87.66±3.0	82.97±2.9	68.92±1.9	68.79±2.0	71.01±2.3	67.76±2.1
w/o Adaptive Logits scaling factor	86.63±2.5	87.27±2.6	85.05±3.1	89.60±2.5	69.66±1.8	69.38±1.9	66.67±2.4	73.83±2.0
MARGIN (Full)	86.87±2.4	87.47±2.5	84.61±3.0	90.52±2.3	71.29±1.7	71.13±1.8	68.39±2.2	75.08±1.9

TABLE IV
SENSITIVITY ANALYSIS OF THE BASE SCALING FACTOR s_0 ON BIGVUL.

s_0	Binary F1 (%)	CWE-Macro F1 (%)
5	86.56	69.50
10	85.98	63.78
15	87.38	70.09
20	87.35	71.22
25	86.66	69.32
30	87.45	67.82
35	87.37	70.12
40	87.14	68.18
45	86.86	70.10
50	85.98	68.40
55	85.25	68.79
60	85.00	69.01

latency is **111–125 ms** per sample, measured with a batch size of 1 on a single NVIDIA A100 GPU with 40 GB memory. On BigVul, the model typically converges within **10–12 epochs**, after which gains are marginal. Peak GPU memory usage during training is around 12 GB, well within industrial capacity.

Given these measurements, the computational cost of MARGIN is considered acceptable for industrial deployment under typical resource and latency constraints.

VII. CASE STUDY

We use the BigVul dataset as a case study. Motivated by our analysis, we examine training dynamics and key metrics to show why our model remains effective under class imbalance.

Per-CWE Performance

To evaluate the classification performance of our method across different classes, we present the per-CWE F1 performance, examining how classes with varying frequencies are classified. This allows us to verify the robustness of our method under extreme class imbalance.

Figure. 6 illustrates the per-class F1 scores in relation to the support (number of samples) for various CWE types, providing a detailed view of how each method copes with class imbalance. A clear pattern emerges from the visualization: while baseline methods exhibit considerable volatility that correlates with sample size, the proposed MARGIN method (depicted as a solid green line) demonstrates remarkable stability and robustness across all classes. Unlike the baselines, MARGIN consistently achieves high F1 scores—generally above 60%—showing minimal sensitivity to fluctuations in support, as indicated by the grey bars.

The advantages of MARGIN are particularly pronounced in long-tail scenarios, where data scarcity presents a signif-

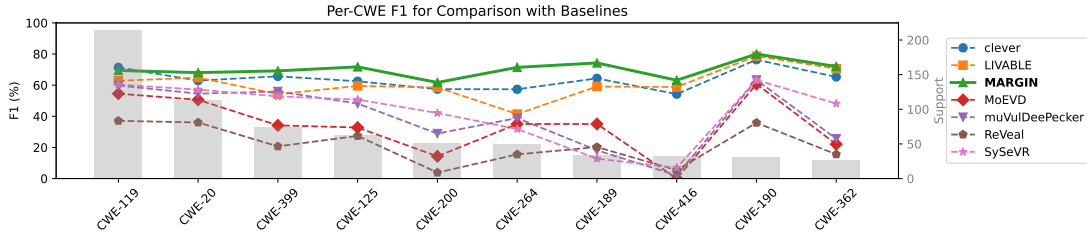


Fig. 6. **Per-CWE F1 Performance Comparison with Baselines** Per-class F1 scores and support for MARGIN and baseline methods across different CWE categories. The bar chart indicates the number of samples per class (support), while the line plots represent F1 scores. MARGIN is highlighted with a red solid line to emphasize its performance.

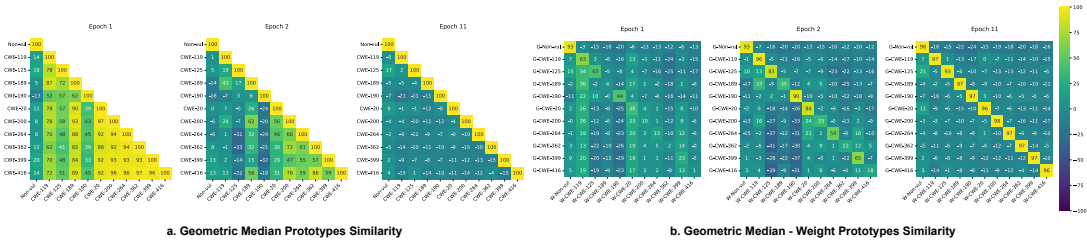


Fig. 7. **Prototypes Convergence During the Training Epochs.** Guided by the adaptive margin mechanism, the geometric median prototypes are not only mutually separated but also aligned with the weight prototypes, suggesting that the embedding distributions of different classes gradually form a clear, separable, and stable structure.

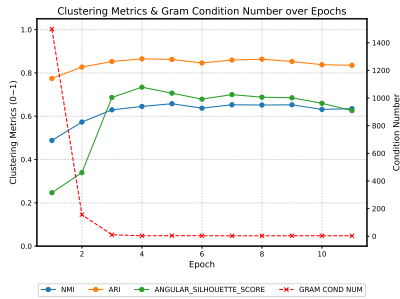


Fig. 8. **Clustering and ETF Dynamics** During training, NMI, ARI, angular silhouette, and the Gram condition number of geometric median prototypes change rapidly at first and stabilize later, demonstrating our method’s effectiveness in achieving a well-structured, stable prototype configuration.

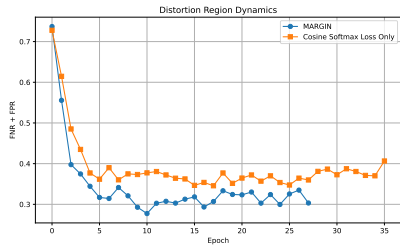


Fig. 9. **Distortion Region Dynamics** Comparison of Macro FNR + Macro FPR across training epochs. MARGIN consistently yields lower error rates than cosine softmax, indicating reduced distortion region effects and improved robustness under class imbalance.

icant challenge. For example, in CWE-416, which exhibits extreme imbalance with very few samples, most competing methods such as *reveal*, *moevd*, and *mvd* suffer dramatic performance degradation, with F1 scores approaching zero. In contrast, MARGIN maintains a robust F1 of approximately

60%, indicating its ability to learn discriminative features even in severely underrepresented classes. Moreover, while methods like *clever* and *livable* achieve competitive peaks in high-support classes (e.g., CWE-190), they display notable instability in medium-support categories such as CWE-200 and CWE-189. MARGIN, however, preserves a steady performance across the spectrum, demonstrating that it does not merely overfit to head classes but generalizes effectively to both frequent and rare vulnerability types.

Structure Convergence

Our method learns embeddings on the unit hypersphere. To examine the geometric structure during training, we conducted a per-epoch dynamic analysis across three dimensions: class concentration (via κ statistics), prototype convergence (toward ETF), and global cluster structure.

Figure 7(a) shows that on BigVul, geometric median prototypes initially fluctuate but rapidly diverge and stabilize, indicating effective class separation. Figure 7(b) reveals that class weight prototypes progressively align with their geometric medians, confirming that the adaptive margin mechanism simultaneously enhances inter-class separation and intra-class compactness.

Figure 8 tracks the first 11 epochs, with clustering metrics (NMI, ARI, Angular Silhouette) on the left axis and the Gram matrix condition number for geometric median prototypes on the right. All metrics rise sharply in early epochs, then plateau around epoch 4, signaling rapid convergence to a discriminative feature space towards the ETF structure. Notably, ARI reaches the highest value, indicating strong agreement with ground-truth assignments. Concurrently, the condition number plummets from > 1400 to near 1 and remains low, marking a transition from ill-conditioned, highly correlated prototypes to a numerically stable, well-spread configuration with uniform

angular distances—hallmarks of an ETF.

These results demonstrate that the learned prototypes rapidly self-organize into a stable, maximally separated structure, providing empirical validation that the adaptive mechanisms effectively enforce embedding space uniformity.

Distortion Elimination

As discussed in our earlier section III, the distortion region refers to the phenomenon where the probability mass of one class intrudes into the Voronoi cells of other classes, directly leading to increases in global macro FNR and FPR. Our adaptive margin mechanism explicitly aims to reduce these distortion regions and thereby improve classification accuracy. The figure below illustrates the dynamics of the global macro FNR and FPR across training epochs. For comparison, we also show results obtained without the adaptive mechanism, using only the Cosine Softmax Loss, highlighting the effectiveness of our adaptive margin in mitigating distortion regions.

Due to computational constraints, precisely quantifying the distortion region on the unit hypersphere is infeasible. However, as discussed earlier, it is closely related to FPR and FNR, allowing us to estimate its size indirectly by analyzing these metrics for each class.

We compare MARGIN with a variant that removes the adaptive mechanism, relying solely on the cosine softmax loss (Figure 9). Even at later training stages, the cosine softmax loss exhibits relatively high FPR and FNR, whereas MARGIN significantly reduces both. This suggests the adaptive mechanism reduces distortion across classes and improves alignment within each region, thereby enhancing robustness under class imbalance.

VIII. RELATED WORKS

A. Representation Learning

Code representation learning aims to map programs into continuous embedding spaces for downstream tasks such as vulnerability detection and code search. Early approaches, such as Code2Vec [6], rely on token- or path-based representations and largely overlook global structural dependencies.

Graph-based methods, including MGVD [24] and Deyign [25], incorporate structural information from ASTs, CFGs, and data-flow graphs, improving semantic expressiveness at the cost of higher computational complexity.

More recently, Transformer-based pre-trained models, such as CodeBERT [26], GraphCodeBERT [27], CodeT5 [28], and UniXCoder [29], have become the dominant paradigm due to their strong transferability. However, existing work mainly evaluates representations via aggregate performance metrics, with limited analysis of embedding-space geometry and class-wise distributional properties.

B. Metric Learning

Metric learning enhances representations by enforcing intra-class compactness and inter-class separability. Early pairwise or triplet losses are sensitive to sampling [30], while margin-based Softmax variants, such as ArcFace [31], introduce angular margins under hyperspherical constraints to improve open-set recognition [1], [32]. These methods apply fixed,

sample-level margins to enlarge class separation. Moreover, it focus on open-set recognition and do not explicitly address class imbalance, whereas our work targets the closed-set, imbalanced scenario.

Unlike margin-based methods, our approach does not treat the margin as a tunable parameter. We model class-conditional distributions on the hypersphere and derive constraints from their geometric misalignment with Voronoi decision regions, directly regularizing the embedding geometry at the class level. While superficially similar to ArcFace-style formulations, the resulting separation emerges naturally from the global class structure rather than manually designed, sample-level margins.

C. Imbalanced Classification Learning

Class imbalance remains a major challenge in vulnerability detection. Conventional methods, such as Weighted Cross-Entropy, Focal Loss, and Class-Balanced Loss [1], [2], mitigate imbalance through re-weighting strategies, but generally assume homogeneous intra-class distributions and lack explicit geometric [2], [4], [30], [33].

Recent work explores prototype learning and metric-space regularization to improve minority discrimination. However, such geometry-aware approaches remain underexplored in software vulnerability detection.

Existing studies typically treat representation learning, metric learning, and imbalance handling as separate problems. In contrast, multi-CWE vulnerability detection requires jointly addressing semantic heterogeneity, long-tailed distributions, and embedding geometry. Our work unifies these aspects by integrating hyperspherical modeling, adaptive margins, and prototype-based learning into a single framework.

IX. CONCLUSION AND FUTURE WORK

We study vulnerability detection under realistic, highly imbalanced CWE distributions from an embedding geometry perspective. By regularizing the hyperspherical structure of representations, our method enhances class separability and decision boundary stability, achieving consistent gains over strong baselines while providing a geometrically interpretable, imbalance-aware framework.

Evaluation is limited to C/C++ due to dataset availability, and generalization to other languages remains untested. Results may be influenced by stochastic factors, though improvements are consistent. Future work will focus on enhancing representation learning to better handle class imbalance, improve feature discriminability for rare CWEs, and enable more robust detection across diverse distributions.

DATA AND CODE AVAILABILITY

The source code, dataset, and full pipelines are available at <https://github.com/stratum-dev/MARGIN> for reproducibility.

ACKNOWLEDGMENT

The authors thank their colleagues and reviewers for their valuable feedback. AI-assisted tools were used solely for language polishing, without influencing any technical content or scientific results.

REFERENCES

- [1] J. Terven, D.-M. Cordova-Esparza, J.-A. Romero-González, A. Ramírez-Pedraza, and E. Chávez Urbiola, "A comprehensive survey of loss functions and metrics in deep learning," *Artificial Intelligence Review*, vol. 58, 04 2025.
- [2] Y. Guo, Q. Hu, Q. Tang, and Y. L. Traon, "An empirical study of the imbalance issue in software vulnerability detection," in *Computer Security – ESORICS 2023*, G. Tsudik, M. Conti, K. Liang, and G. Smaragdakis, Eds. Cham: Springer Nature Switzerland, 2024, pp. 371–390.
- [3] F. Li, J. Luo, F. Peng, Y. Qian, H. Yan, and Z. Zhu, "Neural collapse to multiple centers for imbalanced data," in *Advances in Neural Information Processing Systems 37*, ser. NeurIPS 2024. Neural Information Processing Systems Foundation, Inc. (NeurIPS), 2024, p. 65583–65617. [Online]. Available: <https://dx.doi.org/10.52202/079017-2095>
- [4] Y. Cui, M. Jia, T.-Y. Lin, Y. Song, and S. Belongie, "Class-balanced loss based on effective number of samples," in *2019 IEEE/CVF Conference on Computer Vision and Pattern Recognition (CVPR)*. IEEE, Jun. 2019, p. 9260–9269. [Online]. Available: <https://dx.doi.org/10.1109/cvpr.2019.00949>
- [5] Y. Guo and S. Bettaieb, "An investigation of quality issues in vulnerability detection datasets," in *2023 IEEE European Symposium on Security and Privacy Workshops (EuroS&PW)*. IEEE, Jul. 2023, p. 29–33. [Online]. Available: <https://dx.doi.org/10.1109/eurospw59978.2023.00008>
- [6] U. Alon, M. Zilberstein, O. Levy, and E. Yahav, "Code2vec: Learning distributed representations of code," *Proc. ACM Program. Lang.*, vol. 3, no. POPL, pp. 40:1–40:29, Jan. 2019. [Online]. Available: <https://doi.acm.org/10.1145/3290353>
- [7] S. Geman, E. Bienenstock, and R. Doursat, "Neural networks and the bias/variance dilemma," *Neural Computation*, vol. 4, no. 1, p. 1–58, Jan. 1992. [Online]. Available: <https://dx.doi.org/10.1162/neco.1992.4.1.1>
- [8] P. Mettes, E. van der Pol, and C. G. M. Snoek, "Hyperspherical prototype networks," in *Advances in Neural Information Processing Systems*, 2019.
- [9] R. Ranjan, C. D. Castillo, and R. Chellappa, "L2-constrained softmax loss for discriminative face verification," *ArXiv*, vol. abs/1703.09507, 2017. [Online]. Available: <https://doi.org/10.48550/arXiv.1703.09507>
- [10] E. Markou, T. Ajanthan, and S. Gould, "Guiding neural collapse: Optimising towards the nearest simplex equiangular tight frame," in *NeurIPS*, 2024.
- [11] A. Banerjee, I. S. Dhillon, J. Ghosh, and S. Sra, "Clustering on the unit hypersphere using von mises–fisher distributions," in *Journal of Machine Learning Research*, vol. 6, 2005, pp. 1345–1382.
- [12] C. Lampert, M. Mondelli, and P. Šukeník, "Deep neural collapse is provably optimal for the deep unconstrained features model," in *Advances in Neural Information Processing Systems 36*, ser. NeurIPS 2023. Neural Information Processing Systems Foundation, Inc. (NeurIPS), 2023, p. 52991–53024. [Online]. Available: <https://dx.doi.org/10.52202/075280-2306>
- [13] S. Gopal and Y. Yang, "Von mises-fisher clustering models," in *Proceedings of the 31st International Conference on Machine Learning*, ser. Proceedings of Machine Learning Research, E. P. Xing and T. Jebara, Eds., vol. 32, no. 1. Beijing, China: PMLR, 22–24 Jun 2014, pp. 154–162. [Online]. Available: <https://proceedings.mlr.press/v32/gopal14.html>
- [14] J. Fan, Y. Li, S. Wang, and T. N. Nguyen, "A c/c++ code vulnerability dataset with code changes and cve summaries," in *2020 IEEE/ACM 17th International Conference on Mining Software Repositories (MSR)*, 2020, pp. 508–512.
- [15] C. Ni, L. Shen, X. Yang, Y. Zhu, and S. Wang, "Megavul: A c/c++ vulnerability dataset with comprehensive code representations," in *Proceedings of the 21st International Conference on Mining Software Repositories*, ser. MSR '24. New York, NY, USA: Association for Computing Machinery, 2024, p. 738–742. [Online]. Available: <https://doi.org/10.1145/3643991.3644886>
- [16] X. Wang, R. Hu, C. Gao, X.-C. Wen, Y. Chen, and Q. Liao, "Reposvul: A repository-level high-quality vulnerability dataset," in *Proceedings of the 2024 IEEE/ACM 46th International Conference on Software Engineering: Companion Proceedings*, ser. ICSE-Companion '24. New York, NY, USA: Association for Computing Machinery, 2024, p. 472–483. [Online]. Available: <https://doi.org/10.1145/3639478.3647634>
- [17] S. Chakraborty, R. Krishna, Y. Ding, and B. Ray, "Deep learning based vulnerability detection: Are we there yet?" *IEEE Transactions on Software Engineering*, vol. 48, no. 9, p. 3280–3296, Sep. 2022. [Online]. Available: <https://dx.doi.org/10.1109/tse.2021.3087402>
- [18] X.-C. Wen, C. Gao, F. Luo, H. Wang, G. Li, and Q. Liao, "Livable: Exploring long-tailed classification of software vulnerability types," *IEEE Transactions on Software Engineering*, vol. 50, no. 6, p. 1325–1339, Jun. 2024. [Online]. Available: <https://dx.doi.org/10.1109/tse.2024.3382361>
- [19] D. Zou, S. Wang, S. Xu, Z. Li, and H. Jin, "μvuldeepecker: A deep learning-based system for multiclass vulnerability detection," *IEEE Transactions on Dependable and Secure Computing*, vol. 18, no. 5, pp. 2224–2236, 2021.
- [20] Z. Li, D. Zou, S. Xu, H. Jin, Y. Zhu, and Z. Chen, "Sysevr: A framework for using deep learning to detect software vulnerabilities," *IEEE Transactions on Dependable and Secure Computing*, vol. 19, no. 4, p. 2244–2258, Jul. 2022. [Online]. Available: <https://dx.doi.org/10.1109/tdsc.2021.3051525>
- [21] C. Ji, S. Yang, H. Sun, and Y. Zhang, "Applying contrastive learning to code vulnerability type classification," in *Conference on Empirical Methods in Natural Language Processing*, 2024. [Online]. Available: <https://api.semanticscholar.org/CorpusID:273901675>
- [22] X. Yang, S. Wang, J. Zhou, and W. Zhu, "One-for-all does not work! enhancing vulnerability detection by mixture-of-experts (moe)," *Proceedings of the ACM on Software Engineering*, vol. 2, no. FSE, p. 446–464, Jun. 2025. [Online]. Available: <https://dx.doi.org/10.1145/3715736>
- [23] J. Li, L. Cui, S. Zhao, Y. Yang, L. Li, and H. Zhu, "Clever: Multi-modal contrastive learning for vulnerability code representation," in *Findings of the Association for Computational Linguistics: ACL 2025*. Association for Computational Linguistics, 2025, p. 7940–7951. [Online]. Available: <https://dx.doi.org/10.18653/v1/2025.findings-acl.414>
- [24] F. Qiu, Z. Liu, X. Hu, X. Xia, G. Chen, and X. Wang, "Vulnerability detection via multiple-graph-based code representation," *IEEE Transactions on Software Engineering*, vol. 50, no. 8, p. 2178–2199, Aug. 2024. [Online]. Available: <https://dx.doi.org/10.1109/tse.2024.3427815>
- [25] Y. Zhou, S. Liu, J. Siow, X. Du, and Y. Liu, *Devign: effective vulnerability identification by learning comprehensive program semantics via graph neural networks*. Red Hook, NY, USA: Curran Associates Inc., 2019.
- [26] Z. Feng, D. Guo, D. Tang, N. Duan, X. Feng, M. Gong, and M. Zhou, "Codebert: A pre-trained model for programming and natural languages," in *Findings of the Association for Computational Linguistics: EMNLP 2020*, 2020, pp. 1536–1547. [Online]. Available: <https://dx.doi.org/10.18653/v1/2020.findings-emnlp.139>
- [27] D. Guo, S. Ren, S. Lu, Z. Feng, D. Tang, S. Liu, L. Zhou, N. Duan, A. Svyatkovskiy, S. Fu, M. Tufano, S. K. Deng, C. B. Clement, D. Drain, N. Sundaresan, J. Yin, D. Jiang, and M. Zhou, "Graphcodebert: Pre-training code representations with data flow," in *ICLR*. OpenReview.net, 2021. [Online]. Available: <https://dblp.uni-trier.de/db/conf/iclr/iclr2021.html#GuoRLFTOZDSFTDC21>
- [28] Y. Wang, W. Wang, S. Joty, and S. C. Hoi, "Codet5: Identifier-aware unified pre-trained encoder-decoder models for code understanding and generation," in *Proceedings of the 2021 Conference on Empirical Methods in Natural Language Processing*. Association for Computational Linguistics, 2021, p. 8696–8708. [Online]. Available: <https://dx.doi.org/10.18653/v1/2021.emnlp-main.685>
- [29] D. Guo, S. Lu, N. Duan, Y. Wang, M. Zhou, and J. Yin, "Unixcoder: Unified cross-modal pre-training for code representation," in *Proceedings of the 60th Annual Meeting of the Association for Computational Linguistics (Volume 1: Long Papers)*. Association for Computational Linguistics, 2022, p. 7212–7225. [Online]. Available: <https://dx.doi.org/10.18653/v1/2022.acl-long.499>
- [30] X. Yang, S. Wang, Y. Li, and S. Wang, "Does data sampling improve deep learning-based vulnerability detection? yeas! and nays!" in *Proceedings of the 45th International Conference on Software Engineering*, ser. ICSE '23. IEEE Press, 2023, p. 2287–2298. [Online]. Available: <https://doi.org/10.1109/ICSE48619.2023.00192>
- [31] J. Deng, J. Guo, N. Xue, and S. Zafeiriou, "Arcface: Additive angular margin loss for deep face recognition," in *2019 IEEE/CVF Conference on Computer Vision and Pattern Recognition (CVPR)*, 2019, pp. 4685–4694.
- [32] Y. Meng, J. Huang, G. Wang, C. Zhang, H. Zhuang, L. Kaplan, and J. Han, *Spherical text embedding*. Red Hook, NY, USA: Curran Associates Inc., 2019.
- [33] Y. He, G. Lin, X. Ma, J. W. Keung, C. Tan, W. Hu, and F. Li, "Enhancing deep learning vulnerability detection through imbalance loss functions: An empirical study," *Proceedings of the 15th Asia-Pacific Symposium on Internetware*, 2024. [Online]. Available: <https://api.semanticscholar.org/CorpusID:271293860>